Analytical Hierarchical Process (AHP) Techniques and Geospatial Technologies for Groundwater Potential Zone Mapping

Abstract

Due to its consistent availability, acceptable natural quality, and ease of direct diversion to the underprivileged population, groundwater is a vital source of water supply. It can also be transported there more swiftly and inexpensively. Exploring groundwater potential zones (GWPZs) maps is therefore essential, especially in semi-arid environments with insufficient surface water supplies. The groundwater potential of the research area is assessed using geographic information system methods and remote sensing data. Operational Land Imager 8 data, digital elevation models, soil data, rainfall data, and dug-out-well data were utilized to estimate the characteristics that influence groundwater potential and recharge zones. Maps of lineament density, drainage density, rainfall distribution, topographic-wetness index, land use/land cover, land-surface temperature, slope and soil were produced. These were overlaid based on analytical hierarchical process weightage prioritization at a constituency ratio of 0.05. The resulting map was divided into very high, high, moderate, low and very low groundwater potential zones. The area dimensions of these categories are 116005.5 ha, 35822.4 ha, 20152 ha, 2459 ha and 259245 respectively. Accordingly, the north-east part of the study area is expected to have very high ground□water potential. Out of the 55 operational wells sampled, 72.73 % were situated in areas with very high groundwater potential. The high category had 10.91% while the moderate, low and very low categories remained 7.27%, 5.45% and 3.64% respectively. The overall result indicates that the model approach is reliable and can be adopted for a reliable characterization of GWPZs in any semi-arid/ arid environment.

Keywords: GIS; remote sensing; groundwater potential assessment; analytical hierarchy processes; weight overlay analysis.

Introduction

One-third of all freshwater withdrawals worldwide come from groundwater [1]. In arid and semi-arid nations with limited water supplies, it is an essential natural resource for any economic

growth [2]. Groundwater is a type of water resource that fills joints, voids, and pore spaces in soil found within layers and geologic formations. The presence of groundwater in rocks depends on the lithologic materials' hydraulic conductivity, which is a result of their porosity, permeability, and fluid movement via geologic structures or apertures [3]. The water deficit is a global issue because of the relationship between water, food, and energy and its influence as well as the influence it has on human life and the world economy. Because of the nation's rapid urbanization, population increase, and overall economic growth, Nigeria's need for groundwater is increasing. In the current research region, groundwater is also the most often used resource for residential water supply, agriculture, and livestock. The scarcity of water may persist for a longer period of time in some regions in Nigeria due to the rate at which the population is increasing, the extent to which urbanization and farming activities are reliant on water sources. Things get more challenging due to climate change [4]. Data collection and assessment, the construction of impoundments and water infrastructure for water transfer schemes, water regulations, optimization programmes, and management strategies have all been part of arbitrary efforts to ensure water security [5]. The documentation of groundwater distribution is relatively sketchy [6]. Therefore, the goal of the current research is to increase knowledge of groundwater availability and to give a strategy for mapping groundwater potential zones. Groundwater potential zones (GWPZs) are regions that have a significant amount of commercially exploitable groundwater resources. [7,8]. For the estimation of water resource reserves, zone budgeting, water quality protection, vulnerability mapping, and environmental management, GWPZ exploration is crucial [7]. Various academics across the world have used the RS and GIS techniques to designate groundwater potential zones. [9,10,11]. Geology, geomorphology (landforms), slope, soil type, rainfall, land use, and drainage characteristics are some of the factors that are directly or indirectly related to the research of the location of groundwater potential utilizing RS and GIS [12]. The development of geoscientific data access and processing skills, as well as the numerous geoinformatics applications, have recently made it possible to regionally explore locations with potential for groundwater. A significant improvement has been made as a result of the widespread use of geospatial technology for GWPZ mapping, particularly with the introduction of multi-criteria decision-making (MCDM) statistical classifier [13]. Weight of evidence, evidential belief [14], weighted overlay [15], multi-influencing factors [16], analytical hierarchical process [17,18], logistic regression [19], and frequency ratio are a few examples of statistical tools [20].

The analytical hierarchical process (AHP), among these, has been recognised as the best effective method for making multi-criteria decisions [21]. Machine learning methods (MLT) for resource modelling have been made possible by the development of prediction modelling and the advent of computer programming [22]. MLT's adaptability in the analysis of complex structures and stochastic data has made groundwater resource exploration outcomes more dependable [23,24,25]. In light of this, a number of MLT regression models for GWPZ mapping were suggested. These include boosted regression tree [26,27], support vector machine [28,29],

artificial neural network [30,28], radial basis function, multiple-layer perception, standalone logistic regression [31], and random forest [32,33]. Machine learning techniques are more resilient than unsupervised statistical methods because of their accuracy, speed, ability to process massive databases, and capacity for self-improvement [34]. Additionally, there has been a notable increase in machine learning model performance. For instance, by combining a multi-adaptive boosting model with logistic regression, [35] created the ensemble multi-adoptive boosting logistic regression (MABLR) approach. Due to inadequate sample size, simplicity, and outliers sensitivity, the model offers outstanding performance for groundwater aquifer potential maps for bias and variance error reduction [35]. For the evaluation of groundwater spring potential zones, [36] combined an alternating decision tree classifier with an adaptive boosting ensemble model to create the hybrid computational intelligence technique known as AB-ADTree. In order to map the groundwater potential zone, [37] offer two data mining approaches based on the use of mixed discriminant analysis and linear discriminant analysis (LDA) in comparison with random forest. By normalizing the 15 conditioning factors in the variance inflation factor, chi-square factor optimization, and Gini importance, the duplication within the groundwater conditioning factors was reduced. Their findings showed that, despite the random forest approach's superior performance, the two data mining strategies are acceptable and moderate [37]. Additionally, [38] created a hybrid method for measuring the potential of groundwater springs that combines Fisher's LDA, rotation forest LDA, and bagging LDA. The ensemble learning model and MLT's meta-algorithm compartment, which make it easier to do multivariate analysis on a large dataset, both increase the computing power of MLT [25]. While the skewness and operational complexity of MCDM statistics rise with the increase in unpredictability and sample size, MLT works by scientifically improving itself as sample distribution, sizes, and randomness increase [34]. Seven datasets are utilised in this study to evaluate their suitability for site-specific GWPZ investigation. AHP was used as the statistical classifier since this study is more research-oriented than result-oriented. According to [39], there are boreholes in the west of the research area that have been abandoned owing to the mechanical failure of the borehole hardware. [39] also evaluated the variables impacting the underdevelopment of groundwater and inadequate management of groundwater boreholes. The assessment of groundwater potential zones based on the accumulation of statistically weighted geoscientific layers within the research region is the main topic of the current work. In order to

determine their weightage prioritization at a catchment scale, seven thematic layers were geospatially coordinated using AHP. These include the topographic wetness index (TWI), land use/land cover (LULC), lineament density (LD), drainage density (DD), rainfall distribution (RD), surficial lithology (SL), and land surface temperature (LST). According to the project's goals, it is envisaged that the themes chosen would enhance how AHP is used to an integrated strategy for groundwater investigation. One of the most popular multi-criteria decision-making approaches is the analytical hierarchy process (AHP) approach [40]. In general, AHP is regarded as a straightforward, transparent, efficient, and dependable technique that may be utilized to identify groundwater potential zones [13,41]. Therefore, the purpose of this work is to demonstrate if it is feasible to create a high-precision map of the groundwater potential zone for a semi-arid environment. This strategy's justification is based on the integrated water resources management plan, which promotes the coordinated development of water resources in an environmentally responsible manner [42]. The decision-makers, stakeholders, and the host community at large would all gain greatly from the strategy proposed in this study. The results are supported by the precise yield of the active boreholes and the volume of spring discharge in the targeted locations. The major goal of this project is to map and identify groundwater potential zones utilizing integrated methodologies that promote sustainable planning, development, and use along with effective management of groundwater for drinking and irrigation.

Materials and Methods

Study Area

Oke-Ogun region is the north-western area of Oyo State, and is made up of ten local government areas in the northern and north-western parts of Oyo State, Nigeria. Out of the ten local Government areas, the three largest ones were selected for this study. They are Saki East, Atiba and Orelope local government areas (LGA) (Map 1). It is located between Longitudes $3^{\circ}10'$and $4^{\circ}25'$ and Latitudes $7^{\circ}55'$and $8^{\circ}50'$.The soil types, are Clay loam, Concretionary clay, Loamy fine sand, Sandy soil, Sandy clay, Sandy loam and Silty clay. Rainfall ranges between 646 mm to 673 mm. the geology is basically of the basement complex rocks. The average temperature is about $27^{\circ}C$. The inhabitants are predominantly Yorubas with other tribes like Igbos and

Hausa/Fulanis as minority tribes. Faming and pastoralism are the major economic activities in the study area.

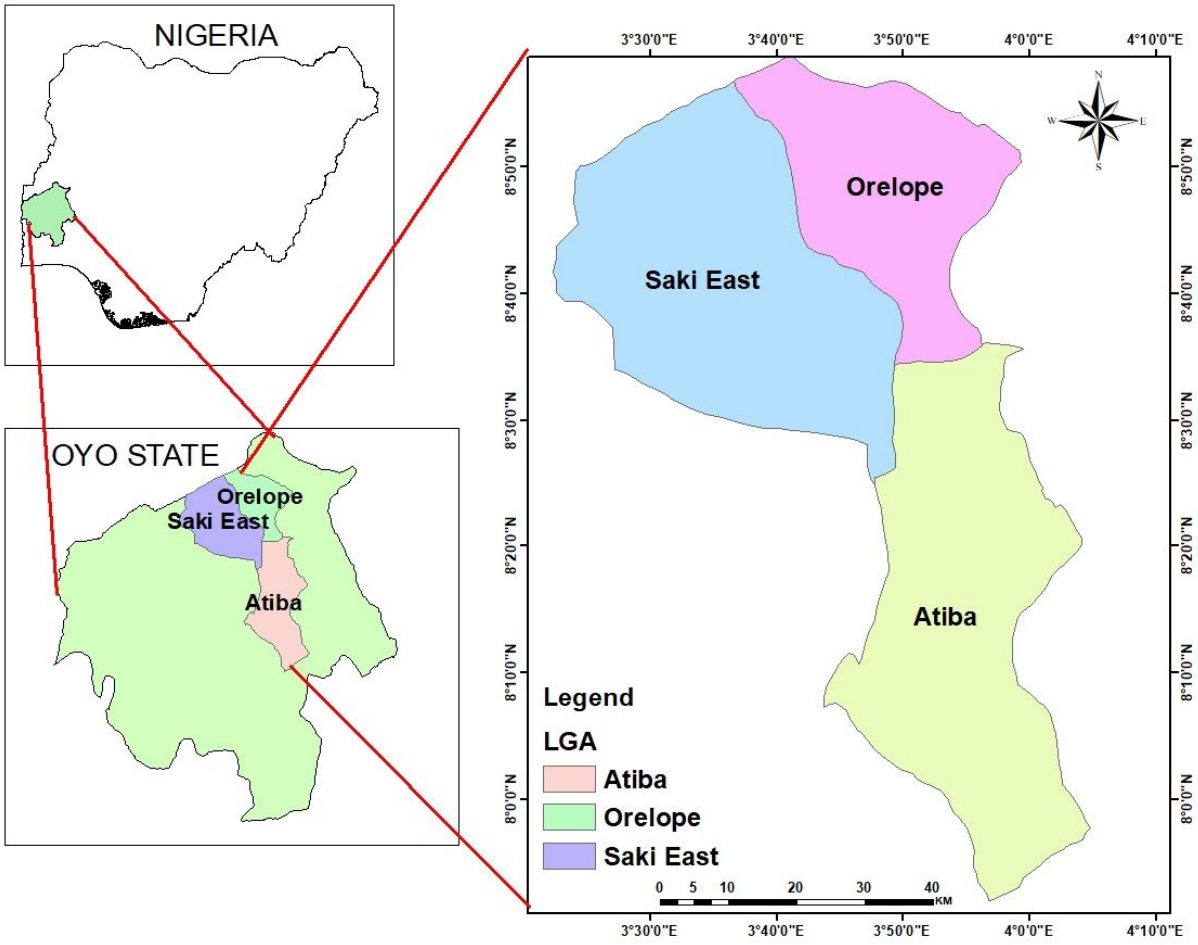

Map 1: Map of the study area

Analytic Hierarchy Process (AHP)

For the purpose of creating the GWPZs map, the current study relies on the compilation of RS and GIS datasets. Nine regulating factors (slope, drainage density, rainfall, lithology, soil characteristics, geomorphology units, land use/land cover, lineament density, and distance to river) were utilized to define the GWPZs. By applying normalized weights to assess the GWPZs of the basin, the AHP approach was used to examine the thematic maps of these parameters. AHP application calls for scientific expertise, credible data, and an evaluation of matrix consistency [43, 44,45]. We applied the AHP approach in a scenario similar to [46] by (i) choosing the factors governing

groundwater recharge, (ii) generating a pairwise comparison matrix, (iii) allocating relative weights, and (iv) assessing the consistency of the matrix (Figure 1).

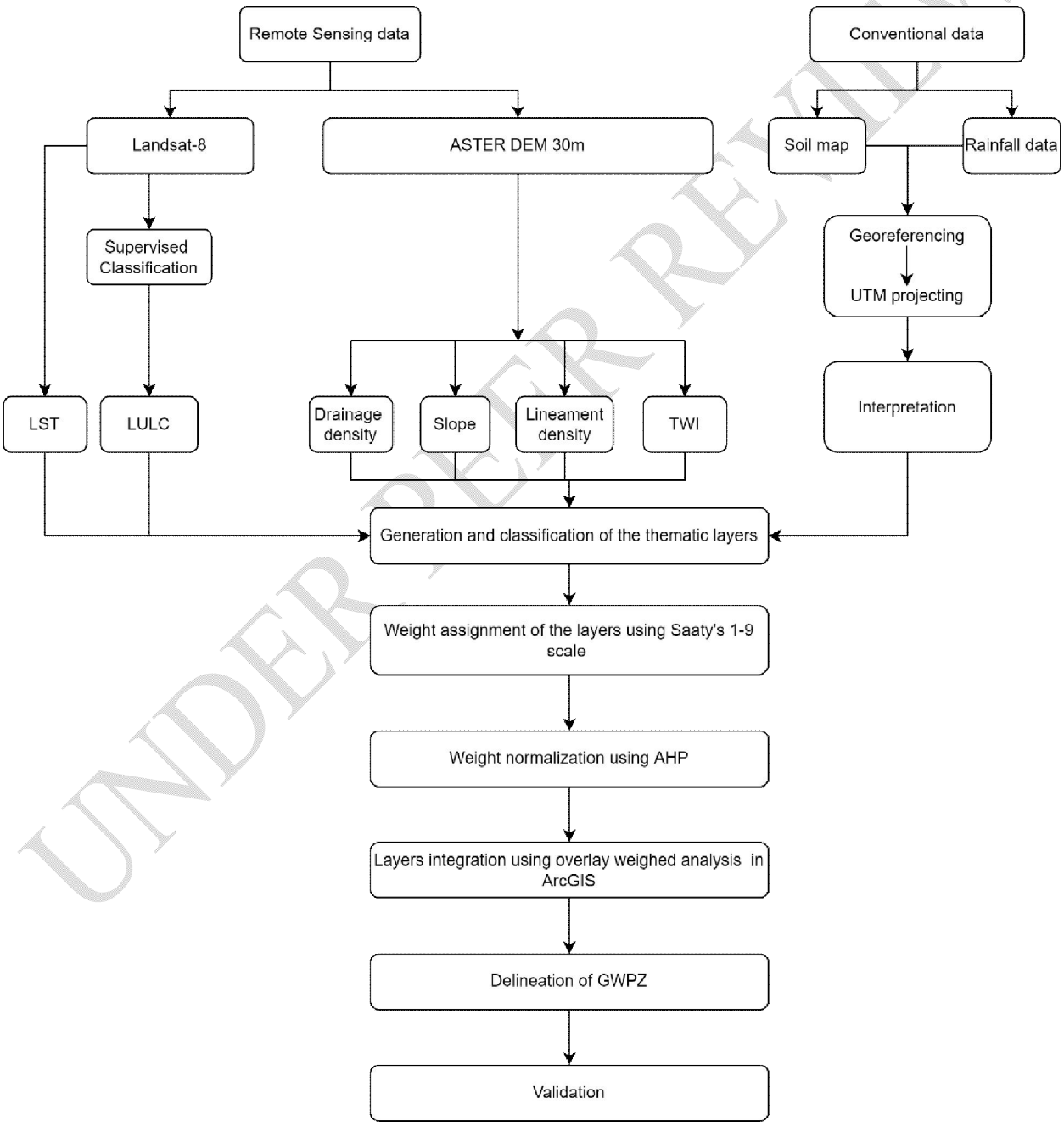

Figure 1: Flow Chart of the methodology adopted for this study

The pair-wise prioritizing method for calculating the weightage of features is made possible by AHP. The characteristic vector of the square reciprocal matrix of paired features serves as the basis for the scoring system for features' weights [47]. AHP has been effectively used in several groundwater potential zone mapping projects as well as environmental management [48,49,50,51,52].

Preparation and computation of the thematic layers

Land surface temperature

The LST theme was created from a download of the Landsat 8 Operational Land Imager from the USGS Earth Explorer website on February 26, 2022. The month is among the driest in the entire year. The satellite data's bands 4, 5, and 10 were processed in the following order:

Equation 1 was used to determine the top of atmospheric (TOA) spectral radiance using raster algebra.

$$TOA = RF_m \times TIRS\,1 + RF_A \quad (1)$$

where

RFM = radiometric multiplicative rescaling factor for TIRS 1 which is 0.0003342,

TIRS = thermal infrared sensor 1 which is Band 10, and

RFA = radiometric addictive rescaling factor for TIRS 1 which is 0.1.

TOA was converted to brightness temperature (BT) using Equation 2

$$BT = \frac{K_1}{\left[ln\left(\frac{K_2}{TOA}\right) + 1\right]} - 273{:}15 \quad (2)$$

where K1 and K2 = Thermal conversion constant for Band 10 extracted from metadata and 273.15 constant for temperature conversion from Kelvin to Celsius.

NDVI was calculated using the expression in Equation 3

$$NDVI = \frac{NIR - RED}{NIR + RED} \quad (3)$$

where NIR (near-infrared) = band 5, and
red = band 4 for Landsat 8 OLI.

Vegetation proportion (P_v) was calculated from NDVI, using Equation 4

$$P_v = \left(\frac{NDVI - NDVI_{min}}{NDVI_{max} - NDVI_{min}}\right)^2 \quad (4)$$

Emissivity was calculated from P_v, using Equation 5

$$\varepsilon = 0.004 \times P_v + 0.986 \quad (5)$$

where

0.004 is the downscaling constant for Pv and

0.986 is the correction value of the equation.

Soil Features

An aquifer's infiltration and percolation rates are significantly influenced by the soil [53]. The vertical and lateral water movement can be significantly impacted by the size, shape, and arrangement of the soil grains and the related pore system [54]. The soil map was downloaded from the Food and Agriculture Organization's (FAO) Geo Network Web Portal for Soil Map (http://www.fao.org/geonetwork/srv/en/metadata.show%3Fid=14116). We obtained information from the "Digital Soil Map of the World—ESRI Shapefile format" section of the FAO website. Additionally, SWAT Soil Data (http://www.indiaremotesensing. com/p/s.html) was used to determine soil classifications. ArcGIS 10.8.2 now includes a soil map that has been georeferenced to the UTM projected coordinate system. Using the tools Analysis Tools > Extract > Clip, we extracted the research area. The soil types on the map were then geo-coded at various category levels in accordance with the classes derived from the SWAT Soil Data.

Rainfall

Rainfall, the primary source of groundwater recharge, has a significant influence in regulating groundwater recharge, according to [55] of the Climate Research Unit (www.cru.uea.ac.uk/data). To get rainfall data, we next chose "Main homepage for the high resolution gridded datasets." Using the tool Multidimensional Tools > Make NetCDF Raster Layer, the rainfall data were transformed into a raster layer. Then, we used the tools Conversion Tools > From Raster > Raster to point to convert the raster layer to points. To create a rainfall contour map, these points were interpolated using the Spatial Analyst Tools > Interpolation > Kriging tool. The Spatial Analyst Tools > Extraction > Obtain by Mask tool was used to extract the rainfall map for the research region. The normal kriging interpolation method and a linear semi-variogram model were used to calculate and estimate the yearly average rainfall in order to create a rainfall themed layer. The resultant rainfall map, which varied geographically, was categorised for overlaying.

Land use/land cover

The map of the land use and land cover was created using ArcGIS 10.8.2, which was used to analyse Landsat 8 OLI data that had less than 10% cloud coverage. The reflectance quality and spectral distortion of the downloaded images were corrected. The LULC was created using this. By creating a composite band from bands 1, 2, 3, 4, 5, 6, and 7, LULC was mapped.

Lineament density

Linear characteristics like fractures, faults, cleavages, and discontinuity surfaces are expressed by lineaments, which are linear properties. When a structure has pieces that are placed in a rectangular or somewhat curved manner, differ from the arrangement of the neighbouring features, or reflect some underlying characteristic, those parts are referred to as a lineament. Lineaments can be simple or complicated. The 30-by-30-meter ASTER DEM was used to create the surface lines. The hydrological algorithm in ArcGIS 10.8.2 was used to do this. High lineament densities are a sign of high permeability zones, which make them suitable locations for GWPZs [56]. Very high, high, moderate, low, and very low lineament density are the most common categories. [57]. After adding the acquired map to ArcGIS, the lineament density was calculated using the tools available under Spatial Analyst Tools > Density > Line Density.

ArcGIS 10.8.2's grid cells approach, which is based on Equation 6, was used to process its density [50]:

$$LD = \sum_{i=1}^{i=n} \left(\frac{L_i}{A}\right) (Km^{-1}) \quad 6$$

where

LD is the lineament density,

L_i is the sum of the length of all the lineaments (km),

i represent each linear feature in the study area, and

A is the effective area of lineament cell grids (km^2).

Drainage density

The total length of all stream segments in a region divided by its area is known as the drainage density [58]. An excellent way to anticipate infiltration rates and highlight the relationship between permeability and surface runoff in terrain is to look at the drainage density [59]. High drainage density terrain has relatively slow recharge rates, whereas low drainage density terrain has faster recharge rates [60]. Poor GWPZ results from high drainage density since they are conducive to runoff, and vice versa [9]. In the current study, the spatial analyst tools > density > line density in ArcGIS 10.4.1 were used to compute the drainage density.

For the purpose of developing drainage density, the USGS Earth Explorer website's ASTER Digital Elevation Model (DEM) was downloaded (DD). The spatial analyzer of ArcGIS was used to create the drainage density map. The delineation of the watershed hydrological pattern is therefore made possible by the calculation of the effective area of drainage. Equation 7 was used to obtain the watershed's drainage density index.

$$DD = \frac{\text{the total length of channels}}{A} \quad 7$$

where

DD means drainage density and

A is the area.

Slope

Groundwater recharge into aquifers is significantly influenced by local and regional relief, which is represented by the slope [61]. The slope gradient, which is frequently utilized in the definition of GWPZs, directly regulates surface water infiltration [62,63]. Due to the greater drainage, an area with a high slope gradient has a comparatively low GWP. However, a low slope gradient restricts water flow, which increases the rate of infiltration [59]. Using the tools found under Spatial Analyst Tools > Surface > Slope in ArcGIS 10.8.2, we calculated the slope after producing the DEM, drainage lines, and watershed border in Section 3.3.

Topographic wetness index

In ArcGIS 10.8.2, the slope map was created from which TWI was mapped. This was accomplished by using Equations 8 and 9 to determine the rate of change of a cell grid aspect within its neighbourhood [64].

$$TWI = In\left[\frac{\alpha}{tan(\beta)}\right] \quad 8$$

$$\alpha = \frac{A}{L} \quad 9$$

Where

$alpha\ is$ the specific catchment area,

A is the catchment area,

L is the contour length, and

tan(β) is the slope.

Slope, elevation, and landform implications on groundwater development were integrated using the TWI map [65]. In this computation, the effects of topographic roughness, hillslope, and

foothill on lateral groundwater flow are combined. The ability to identify areas of soil moisture storage and infiltration potential unique to foothills is made possible by locations with high TWI [66]. The use of a surficial lithology map in place of a traditional scanned geologic map is a notable feature in the selection of the themes.

List 1: Demographic profile of the study

Factors	Weight	Rank	Over All
Slope			
0-1	20	5	100
1-2		4	80
2-5		3	60
5-14		2	40
14-38		1	20
Rainfall(mm/year)			
646-650	25	4	100
650-659		3	75
659-668		2	50
668-673		1	25
Land Surface Temperature(°C)			
18-24	10	1	10
24-26		2	20
26-29		3	30
29-36		4	40
Drainage Density(km/km^2)			
Very High	15	1	15
High		2	30
Low		3	45
Very Low		4	60
Lineament Density(km/km^2)			
Very High	5	4	20
High		3	15
Low		2	10
Very Low		1	5
TWI			
Very High	5	4	225
High		3	170
Low		2	10
Very Low		1	5
Soil			
Clay-Loam		8	120
Concretionary Clay		4	60

Loamy Fine Sand	15	7	105
Sandy		6	90
Sandy-Clay		3	45
Sandy-Loam		5	75
Silty-Clay		1	15
LULC			
Bare Land	5	1	5
Light Forest		2	10
Thick Forest		3	15
Water Body		4	20

Table 1. Groundwater potential prospect rainfall map classes

Rainfall Classes(mm)	Value (Rank)	GWP Prospect Rank
646-650	1	Very Low
650-659	2	Low
659-668	3	High
668-673	4	Very High

Table 2. Groundwater potential prospect reclassified slope map information.

Slope Classes (Degree)	Value (Rank)	GWP Prospect Rank
27.7–75.9	1	Very Low
17.9–27.7	2	Low
10.4–17.9	3	Moderate
4.5–10.4	4	High
0–4.5	5	Very High

Table 3. Groundwater potential prospect reclassified drainage density map information

DD Classes (km/km^2)	Value (Rank)	GWP Prospect Rank
1.3-1.8	1	Very Low
0.7-1.3	2	Low
0.4-0.7	3	High
0-0.4	4	Very High

Table 4. Groundwater potential prospect reclassified lineament density map information.

LD Classes (km/km^2)	Value (Rank)	GWP Prospect Rank
0-0.4	1	Very Low
0.4-0.8	2	Low
0.8-1.6	3	High
1.6-2.7	4	Very High

Table 5. Groundwater potential prospect reclassified LULC map information.

Class Name	Value (Rank)	GWP Prospect Rank
Bare Land	1	Very Low
Light Forest	2	Low
Thick Forest	3	High
Water Body	4	Very High

Table 6. Groundwater potential prospect reclassified LST map information.

LST Classes	Value (Rank)	GWP Prospect Rank
18-24	1	Very Low
24-26	2	Low
26-29	3	High
29-36	4	Very High

Table 7. Groundwater potential prospect reclassified TWI map information.

TWI Classes	Value (Rank)	GWP Prospect Rank
	1	Very Low
	2	Low
	3	High
	4	Very High

Multi-criteria decision analysis using GIS techniques.

The most popular and well-known GIS-based approach for defining groundwater potential zones is multi-criteria decision analysis utilising Analytical Hierarchical Process (AHP). This approach facilitates the fusion of all topic levels. For this study, a total of 12 distinct theme levels were taken into account. The area's water flow and storage are supposedly under the direction of these 12 thematic strata. According to the relationship between these contributing elements and professional judgement, groundwater occurrence is given more weight. A high weight value shows a layer with a large impact, while a low weight parameter shows a layer with little impact on groundwater potential. Each parameter's weights were determined using Saaty's scale of relative relevance values (1–9).

Table 8: Saaty’s Scale for Assignment and its Interpretation showing Pair-Wise Comparison process [67,49].

Less important	Extremely	9
	Very Strongly	7
	Strongly	5
	Moderately	3
Equally important	Equally	1
More Important	Moderately	1/3
	Strongly	1/5
	Very strongly	1/7
	Extremely	1/9

2, 4, 6 and 8 are intermediate values.

Additionally, the weights were determined after reviewing earlier research and fieldwork. According to the Saaty scale, a value of 9 denotes extreme importance, 8 indicates very strong importance, 7 indicates very extreme importance, 6 denotes strong importance, 5 indicates strong importance, 4 indicates moderate plus importance, 3 indicates moderate importance, 2 indicates weak importance, and 1 indicates equal importance. According to the categorization, weights are given to the thematic levels depending on their significance. In a pair-wise comparison matrix, all of the thematic layers have thus been compared to one another (Table 9)

Table 9: Pair-wise comparison Matrix

	Rf	Sl	LST	DD	So	LD	TWI	LULC	Normalized Weight
Rf	1.00	4	5	3	2	0.33	5	6	0.25
Sl	0.25	1.00	5	5	3	2	5	0.33	0.15
LST	0.2	0.14	1.00	0.5	0.11	0.14	0.25	0.2	0.02
DD	0.33	0.2	2	1.00	6	0.2	0.33	0.25	0.07
So	0.5	0.33	9	0.17	1.00	3	0.5	0.2	0.16
LD	3	0.5	7	5	0.33	1.00	4	0.5	0.17
TWI	0.2	0.2	4	3	2	0.25	1.00	0.33	0.07
LULC	0.17	3	5	4	5	2	3	1.00	0.18
Total	5.65	9.37	40	21.67	19.44	8.92	19.08	8.81	
						Consistency Index			***0.07***
						Random Index			***1.41***
						Consistency Ratio			***0.05***

Rf = rainfall; Sl = slope; DD = drainage density; So = soil; LULC = land use land cover; LD = lineament density; TWI = Topographic wetness index; LST= Land surface temperature

Computation of the thematic layers' consistency ratio and priority ratings

The proportionate degree of each theme's effect on groundwater development was calculated to increase the groundwater potential zone model's accuracy. A function for the matrix divergence from consistency is represented by the primary characteristic value (λmax) [68]. Only when the consistency ratio is equal to or less than 10% are the assigned weights deemed consistent;

otherwise, these weights must be reevaluated to reduce inconsistency [69]. The consistency metric as shown in Eq. (10) was used to obtain the consistency index:

$$CI = \frac{\lambda_{max^{-n}}}{n-1} \quad 10$$

Where

λ_{max} is the consistency measure and

n is the number of GWPZ factors.

The consistency ratio is calculated using Eq. (11) [67]:

$$CR = \frac{CI}{RCI} \quad 11$$

where

CI is the consistency index based on Eq. 10 and

RCI is the random consistency index obtained from Saaty's 1–9 scale [67].

As long as the consistency ratio is within the anticipated range, the final criterion weights that are produced are regarded as the normalised values. The value of CR is anticipated to fall between 0.01 and 0.09 for a consistent normalisation; otherwise, the priority scores must be modified.

Table 10. Ratio index (RI) for various n scores [67].

N	3	4	5	6	7	8	9	10
CI	0.58	0.89	1.12	1.24	1.32	1.41	1.45	1.49

Analysis of overlays for defining groundwater potential zones

As a summary of the components' actual influences based on their criteria weight to produce the ultimate potential zone, the overlay analysis of the seven thematic layers was performed in ArcGIS 10.5.1. All of the layers' units were rated when they were turned into an integral raster to get at these. Eq. 12 was used to determine the groundwater potential zone.

$$GWPZ = \sum_i^n (X_A \times Y_B) \quad 12$$

where

GWPI is the groundwater potential index,
W_i is the criteria weight,
R_i is the ranking of parameter factors, and
i denotes each of the seven influencing factors with serial number from 1 to 7.

Validation of the prospective zone for groundwater

The National Groundwater Archive of the South African Department of Water Affairs' data on groundwater output from exploratory boreholes was used to validate the designated GWPZs. To filter out the relevant grid code identification of the drill location, the 84 geo-referenced yield data was superimposed on the GWPZ map. To simulate the predicted yield value, the regression equation between the groundwater yield and the distribution diagram of the GWPZ grid codes was determined. Microsoft Excel was used to compute the p-value for the association between the observed value and the simulated value as well as the coefficient of determination (R2), coefficient of correlation (R), and coefficient of correlation (R). Using Eq. (15), R was calculated.

Results and Discussion

Soil

The type of soil formed in an area also plays an important role on groundwater recharge through infiltration and loss through run-off. Sandy soils often allow increased infiltration because of

their higher permeability. The soil map of the study area is classified into seven soil categories, viz., Clay loam, Concretionary clay, Loamy fine sand, Sandy soil, Sandy clay, Sandy loam and Silty clay (Figure 2). Loamy fine sand soils occur in the northeastern parts of the study area, whereas clayey loam soils mostly prevail in the middle areas. Sandy soils have a high percentage of macro pores with faster water infiltration rates compared than loamy soils. Loamy soils which own high percentages of middle size pores have higher infiltration rates than clayey soils which have the highest percentage of fine size pores [70]. Large areas are covered by loam and clayey loam soils and were assigned a high to intermediate priority in groundwater potential analysis. Loamy sand and sandy soils were allocated a very high to extremely high weight.

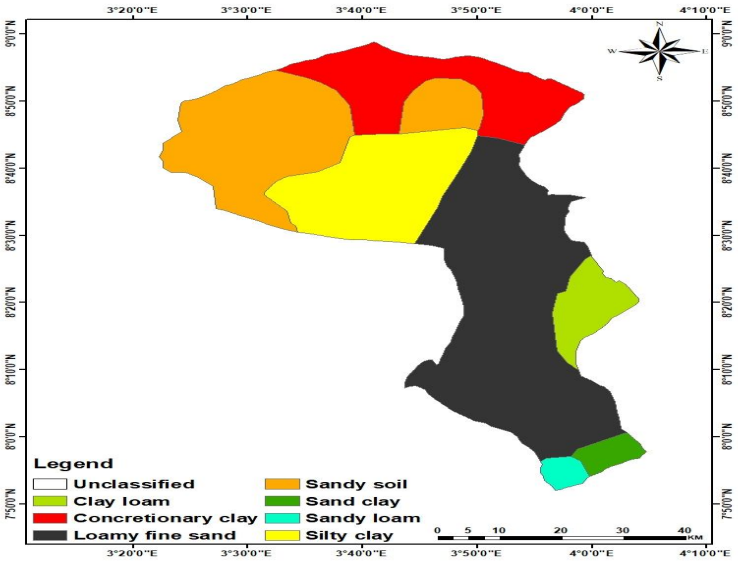

Figure 2: Map of the categories of soil features

Drainage density

The drainage density map was classified into four with areas of high concentration surrounding the river confluence where enormous groundwater discharge to the watercourse. The four spots of high drainage density in the middle and at the North can be associated with the existence of water body. As a result, areas of higher drainage density are inversely ranked while the area of very low drainage density is assigned a higher rank.

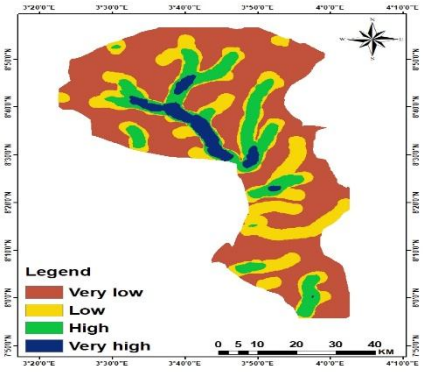

Figure 3: Map of factors of Drainage density

Rainfall map

The spatial variation in rainfall intensity influences the distribution of groundwater recharge rate across the study area. Due to the positive influence of rainfall on groundwater recharge, the areas with higher rainfall range are ranked higher. The overall feature of the mean annual rainfall is that it has the highest levels on the northern parts, of the study area. The five rainfall zones defined in this study are 646 to 650, 650 to 658, 658 to 666, 666 to 667 and 671 to 673 mm yr−1 (Figure 4). The opportunity of groundwater potential and recharge could be excessive in the region where the rainfall is excessive and is low where rainfall is low [71].

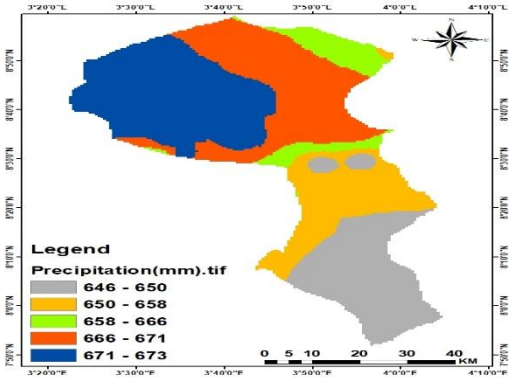

Figure 4: Map of factors of Precipitation

Lineament density map

The lineament density map is classified into five: the very high, high, moderate, and low/none lineament density area (Figure 5). This aligns with the topographic complexity in the North where the relief is steep and abrupt. Areas of extensive fracture system are replicated by high lineament density [72]. Zones of higher lineament density are expected to have higher potential for groundwater accumulation; hence, they are ranked higher. Lineaments, weak zones in the landscape that facilitate the movement of groundwater, are an important theme for GWPZs mapping since they have considerable control over the movement of groundwater [73]. Fractures in rocks enhance their secondary porosity and permeability and thus increase the groundwater movement [74]. Areas with high lineament density in the present study denote permeable zones, so reveal good groundwater potential zones.

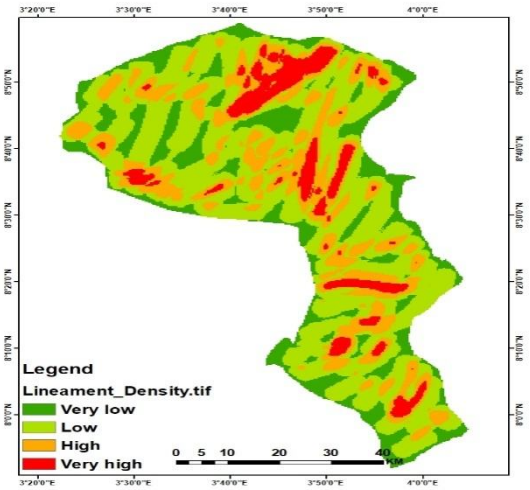

Figure 5: Lineament density map factors

Topographic wetness index

TWI has been employed to decipher the average groundwater level in a watershed characterized by low permeability soils [75]. The very low TWI that suggests the tendency for overland flow was assigned the lowest rank while the very high TWI that indicates the tendency for soil moisture accumulation zone was assigned the highest rank. The TWI showed high concentration in the north and center and coincidence with the drainage density (Figure 6).

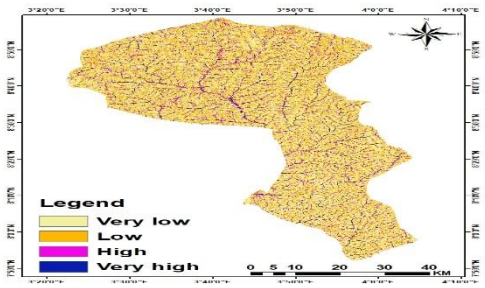

Figure 6: Map showing the factors of TWI

Land use/land cover

The result of the LULC showed four classes, which are bare land, light forest, thick forest and water body. The spatial distribution of the LULC have bare land (146051 ha), light forest (197735 ha), thick forest (78083 ha) and water body (11815 ha) respectively. A mixed forest is a naturally preserved environment and an important indication of groundwater potential. Water bodies, thick forest and light forest are positive indicators of groundwater potential; hence, they are ranked higher than others. Meanwhile, bare land are the least important areas for groundwater investigation. While surfaces protected by vegetation, such as those covered in agricultural plants and forests, have a better chance of groundwater opportunity due to higher infiltration through trapping and protecting the rainwater in plant roots and cracks, bare land and rocky surfaces have much less opportunity of groundwater potential prevalence through growing runoff during rainfall [76,77,78].

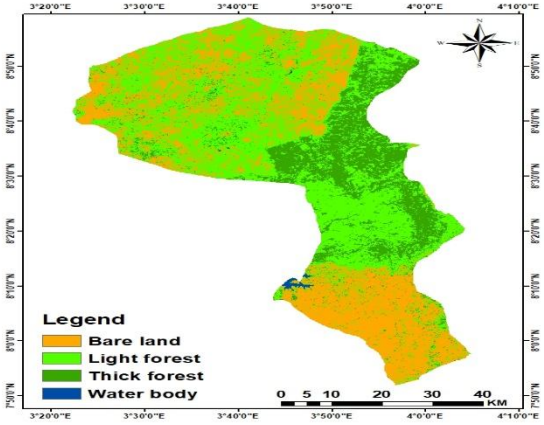

Figure 7: Map showing the factors of LULC

Land surface temperature

The land surface temperature map is classified into four: the very low, low, moderate, and high as presented in Figure 8. Temperature ranges between $18^{\circ}C$ and $36^{\circ}C$. Areas of low temperature had the largest coverage (99109ha), followed by a moderate temperature class (140081ha), the very low-temperature class (75271ha), and the least which is hot temperature class (119223ha). The similitude in the geospatial attributes of LULC and LST further depicts the relative influence of urbanisation in inducing urban heat index which indirectly culminates into the spatial variability in land surface temperature. This, therefore, conforms to the findings of [79] on the relationship between the LULC system and LST variability. Areas of high temperatures are associated with a high evaporation rate. Evaporation is a critical issue in a water-scarce country like Nigeria, where it constitutes a significant soil moisture loss and diminution to shallow unconfined aquifers. As a consequence, areas with high temperatures are assigned the lowest rank while the areas with low temperatures are assigned the highest rank.

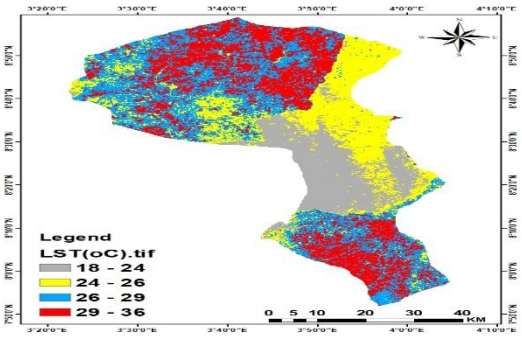

Figure 8: Map showing the factors of Land surface temperature

Delineation of groundwater potential zone

Groundwater is a replenishable resource, but due to various kinds of anthropogenic activities and skewed developments, recharge of this precious life sustaining resource has been reduced significantly. The groundwater availability is not uniform in space and time and therefore, detailed and accurate assessment of the groundwater resource is required. The parameters that

are considered here are slope, rainfall, LULC, LST, lineament density, drainage density, soil, TWI. The weighted overlay method has been applied to generate the groundwater potential zones in the study area. The resulted map is divided into very high, high, moderate, low and very low groundwater potential zones and the aerial spread of these categories are 116005.5 ha, 35822.4 ha, 20152 ha, 2459 ha and 259245 respectively (Figure 9). The study shows that the groundwater potential is high in the north eastern part of the study area and low in the south. The potential groundwater area lies in a perpendicular direction along the West-East direction to the direction of the catchment drainage. Overall, zones with high groundwater potential are dominant in the north-east, while the extremely poor groundwater potential zone is dominant in the south and south. This corresponds to the highly vegetated area of the land use/cover map (Figure 7) and the highly dissected area shown by the drainage density map (Figure 3).

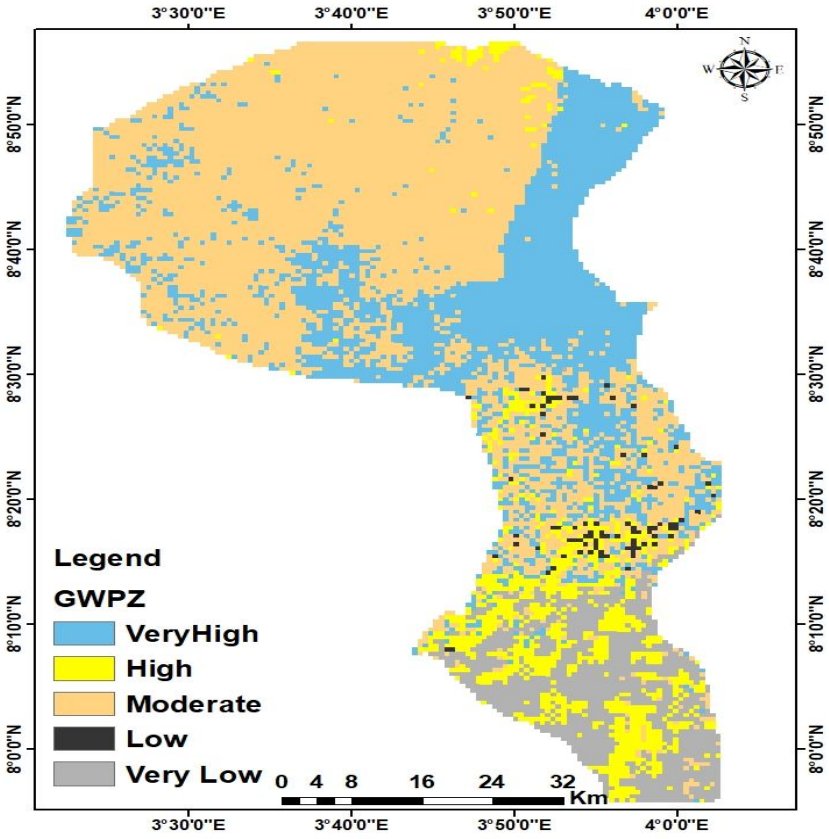

Fig 9: Map showing the Groundwater Potential distribution

Very high and high groundwater potential zones are confined generally to high rainfall regions which in turn have high infiltration potential. The moderate groundwater potential zones occur generally in the valleys and areas of high drainage density.

Ground Water Potential Zone Validation

Since agrarian communities predominate in the study area, borehole drilling remains a privilege reserved for a select group of the communities' elites. As a result, the area's predominantly farming population turned to dug-out wells for home usage, crop irrigation, and small-scale agro-processing. For validation purposes, 43 functional wells were sampled. Our validation will

be limited to the spatial distribution of the sampled wells relative to the categories of the GWPZs because of the absence of available data and the high cost of carrying out the yield capacity of these wells.

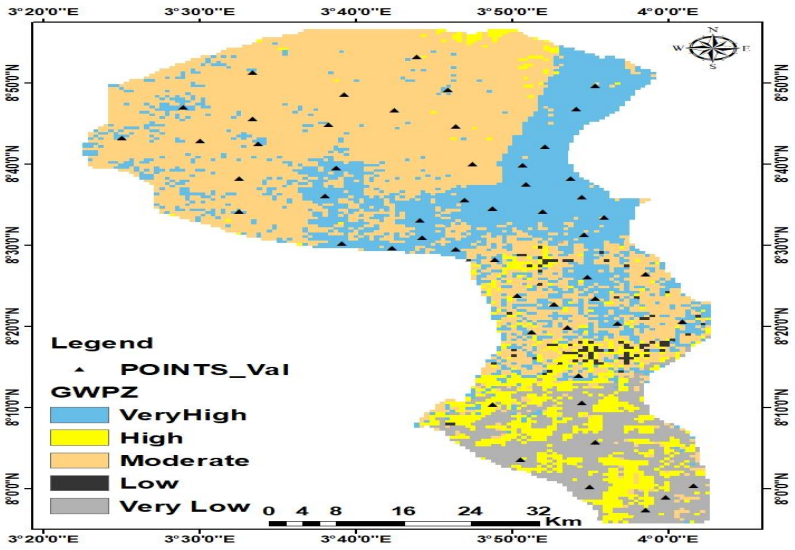

Figure 10: GWPZ map showing the validation points.

Out of the 55 operational wells sampled (Figure 10), 72.73 % were situated in areas with very high groundwater potential. The high category had 10.91% while the moderate, low and very low categories remained 7.27%, 5.45% and 3.64% respectively (Figure 11).

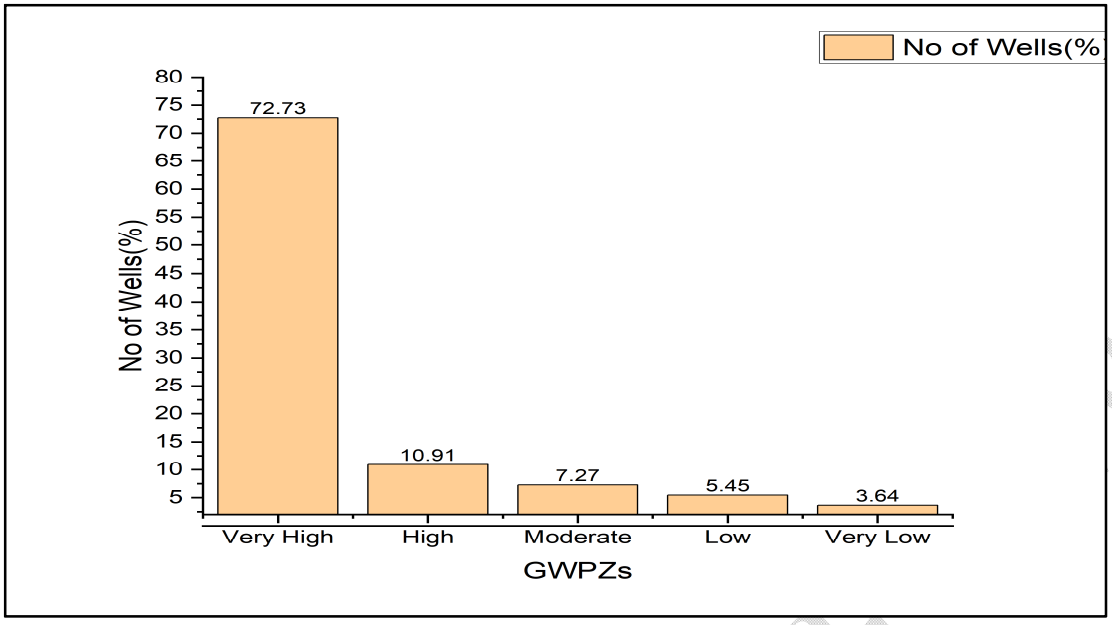

Figure 11: A bar chart showing the spatial distribution of wells in the study area

According to the validation outcomes of the geolocated samples, there may be a very high degree of agreement between groundwater inventory data and groundwater potential zones established using GIS and RS techniques. As a result, it was determined that the results of the weight overlay analysis and the groundwater potential maps supported by the AHP technique were very precise forecasts.

Conclusion

It has been shown how the geosciences technique, which combines geology data with nonlinear, spatially independent environmental, hydrologic, and geomorphic parameters, can be used to map the zones with the greatest potential for groundwater. The work's originality lies in the parameters used and the conceptual processes used to reduce ambiguity and guarantee high precision mapping. From the study, the following findings can be drawn: Overall, the computational method used in this work can be applied to characterize groundwater potential zones and places that need cautious use to prevent groundwater pollution based on the seven factors used in any semi-arid or dry environment with comparable features.

References

1. Taylor G. Richard Scanlon R. Bridget, Doell Petra, Rodell Matthew. Ground Water and Climate Change. Nature Climate Change 2013; 3(4):322-329.
2. Kuisi M. Mustafa, Mashal Kholoud, Al-Qinna I. Mohammed, Abu Hamad M. B. Abdalla. Ground Water Vulnerability and Hazard Mapping in an Arid Region, Case Study, Amman-Zarqa Basin (AZB) Jordan.2014; 6(04):297-318 [CrossRef]
3. Burberry LF, Moore CR, Jones MA, Abraham PM, Humphries BL, Close ME. Study of connectivity of open framework gravel facies in the Canterbury Plains aquifer using smoke as a tracer. Geol Soc Lond, Spec Publ. 2018; 440(1):327–344
4. Owolabi ST, Madi K, Kalumba AM. Comparative evaluation of Spatio-temporal attributes of precipitation and streamflow in Buffalo and Tyume Catchments, Eastern Cape, South Africa. Envir, Devt & Sustl, 2020b; 1–16. [CrossRef]
5. Schreiner B, Hassan R. Transforming water management in South Africa: designing and implementing a new policy framework. Springer Science & Business Media 2, 2010.
6. Cobbing JE, de Wit M. The Grootfontein aquifer: governance of a hydro-social system at Nash equilibrium. South Afr J Sci 2018; 114(5-6): 1–7
7. Waikar ML, Nilawar AP (2014) Identification of groundwater potential zone using remote sensing and GIS technique. Int J Innov Res Sci Eng Tech 2014; 3(5):12163–12174.
8. Thompson SA Hydrology for water management. CRC Press
9. Pinto, D.; Shrestha, S.; Babel, M.; Ninsawat, S. Delineation of groundwater potential zones in the Comoro watershed, Timor Leste using GIS, remote sensing and analytic hierarchy process (AHP) technique. Appl. Water Sci. 2017, 7, 503–519.
10. Das, B.; Pal, S.; Malik, S.; Chakrabortty, R. Modeling groundwater potential zones of Puruliya district, West Bengal, India using remote sensing and GIS techniques. Geol. Ecol. Landsc. 2018, 3, 223–237.
11. Singh, L.K.; Jha, M.K.; Chowdary, V.M. Multi□criteria analysis and GIS modeling for identifying prospective water harvesting and artificial recharge sites for sustainable water supply. J. Clean. Prod. 2017; 142, 1436–1456. [CrossRef]
12. Murasingh. Analysis of Groundwater Potential Zones Using Electrical Resistivity: Remote Sensing and GIS Techniques in a Typical Mine Area of Odisha; National Institute of Technology: Rourkela, India. 2018.
13. Machiwal, D.; Madan, K.; Jha, M.; Bimal, C.; Mal, B. Assessment of groundwater potential in a semi-arid region of India usingremote sensing, GIS and MCDM techniques. Water Resour. Manag. 2011, 25, 1359–1386. [CrossRef]
14. Tahmassebipoor N, Rahmati O, Noormohamadi F, Lee S. Spatial analysis of groundwater potential using weights-of-evidence and evidential belief function models and remote sensing. Arab J Geosci 2016; 9(1):79
15. Senthilkumar M, Gnanasundar D, Arumugam R. Identifying groundwater recharge zones using remote sensing & GIS techniques in Amaravathi aquifer system, Tamil Nadu, South India. Sust Envir Res J, 2019; 29(1):15. [CrossRef]

16. Anbarasu S, Brindha K, Elango L (2019) Multi-influencing factor method for delineation of groundwater potential zones using remote sensing and GIS techniques in the western part of Perambalur district, southern India. Earth Sci Inf:1–16
17. Sahoo S, Dhar A, Kar A, Ram P. Grey analytic hierarchy process applied to effectiveness evaluation for groundwater potential zone delineation. Geocarto Int 2017; 32(11):1188–1205
18. Sandoval JA, Tiburan CL. Identification of potential artificial groundwater recharge sites in Mount Makiling forest reserve, Philippines using GIS and analytical hierarchy process. Applied Geog 2019; 105:73–85
19. Chen W, Li H, Hou E, Wang S, Wang G, Peng T. GIS-based groundwater potential analysis using novel ensemble weights-of evidence with logistic regression and functional tree models. Sci Total Environ 2018; 634:853–867. [CrossRef]
20. Hong H, Tsangaratos P, Ilia I, Liu J, Zhu AX, Chen W. Application of fuzzy weight of evidence and data mining techniques in the construction of flood susceptibility map of Poyang County, China. Sci Total Environ 2018; 625:575–588
21. Jha MK, Chowdary VM, Chowdhury A. Groundwater assessment in Salboni Block, West Bengal (India) using remote sensing, geographical information system, and multi-criteria decision analysis techniques. Hydrogeol J. 2010; 18(7):1713–1728
22. da Costa KA, Papa JP, Lisboa CO, Munoz R, de Albuquerque VHC. Internet of things: a survey on machine learning-based intrusion detection approaches. Compt Netw, 2019; 151:147–157. [CrossRef]
23. Lee S, Hyun Y, Lee S, Lee M. Groundwater Potential mapping using remote sensing and GIS-based machine learning techniques. Remote Sensing J. 2020; 12(1200)
24. Pourghasemi HR, Sadhasivam N, Yousefi S, Tavangar S, Nazarlou HG, Santosh M. Using machine learning algorithms to map the groundwater recharge potential zones. J Environ Mgmt. 2020; 265:110525
25. Prasad P, Loveson VJ, Kotha M, Yadav R. Application of machine learning techniques in groundwater potential mapping along the west coast of India. GI Sci Remote Sens J. 2020; 1–18
26. Naghibi SA, Pourghasemi HR, Dixon B. GIS-based groundwater potential mapping using boosted regression tree, classification and regression tree, and random forest machine learning models in Iran. Environ Monitoring Assessmt 2016; 188(44)
27. Kordestani MD, Naghibi SA, Hashemi H, Ahmadi K, Kalantar B, Pradhan B. Groundwater potential mapping using a novel data-mining ensemble model. Hydrogeol J. 2019; 27(1):211–224
28. Lee S, Hong SM, Jung HS. GIS-based groundwater potential mapping using artificial neural network and support vector machine models: the case of Boryeong City in Korea. Geocarto Int 2018; 33(8): 847–861
29. Naghibi SA, Pourghasemi HR, Abbaspour K. A comparison between ten advanced and soft computing models for groundwater qanat potential assessment in Iran using R and GIS. Theor Appl Climatol 2018;131:967–984
30. Lee S, Song KY, Kim Y, Park I. Regional groundwater productivity potential mapping using a geographic information system (GIS) based artificial neural network model. Hydrogeol J 2012; 20(8):1511– 1527

31. Pradhan B. Remote sensing and GIS-based landslide hazard analysis and cross-validation using multivariate logistic regression model on three test areas in Malaysia. Adv Space Res 2010; 45(10):1244–1256. [CrossRef]
32. Golkarian A, Naghibi SA, Kalantar B, Pradhan B. Groundwater potential mapping using C5.0, random forest, and multivariate adaptive regression spline models in GIS. Environ Monitoring Assessmt 2018; 190(149)
33. Arabameri A, Rezaei K, Cerda A, Lombardo L, Rodrigo-Comino J. GIS-based groundwater potential mapping in Shahroud Plain, Iran. A comparison among statistical (bivariate and multivariate), data mining, and MCDM approaches. Sci Total Environ 2019; 658: 160–177. [CrossRef]
34. Mueller JP, Massaron L. Machine learning for dummies. John Wiley & Sons. 2016
35. Rizeei HM, Pradhan B, Saharkhiz MA, Lee S. Groundwater aquifer potential modeling using an ensemble multi-adoptive boosting logistic regression technique. J Hydrol 2019; 579:124172
36. Tien Bui D, Shirzadi A, Chapi K, Shahabi H, Pradhan B, Pham BT, Singh VP, Chen W, Khosravi K, Bin Ahmad B, Lee SA. Hybrid computational intelligence approach to groundwater spring potential mapping. Water 2019; 11(10):2013
37. Kalantar B, Al-Najjar HA, Pradhan B, Saeidi V, Halin AA, Ueda N, Naghibi SA. Optimized conditioning factors using machine learning techniques for groundwater potential mapping. Water 2019; 11(9):1909
38. Chen W, Pradhan B, Li S, Shahabi H, Rizeei HM, Hou E, Wang S. Novel hybrid integration approach of bagging-based fisher's linear discriminant function for groundwater potential analysis. Nat Res Research 2019; 28(4):1239–1258
39. Cobbing J. Groundwater for rural water supplies in South Africa. Nelson Mandela Metropolitan University and SLR Consulting (Pty) Ltd, South Africa. 2014
40. Arulbalaji, P. Padmalal D. and Sreelash K. GIS and AHP Techniques Based Delineation of Groundwater Potential Zones: a case study from Southern Western Ghats, India. *Scientific Reports* 2019; 9:2082
41. Patra, S.; Mishra, P.; Mahapatra, S. Delineation of groundwater potential zone for sustainable development: A case study from Ganga Alluvial Plain covering Hooghly district of India using remote sensing, geographic information system and analytic hierarchy process. J. Clean. Prod. 2018, 172, 2485–2502
42. Cosgrove WJ, Loucks DP. Water management: current and future challenges and research directions. Water Res Res 2015; 51(6):4823–4839
43. Riad, P.; Billib, M.; Hassan, A.; Salam, M.A.; El Din, M.N. Application of the overlay weighted model and boolean logic to determine the best locations for artificial recharge of groundwater. J. Urban Environ. Eng. 2011, 5, 57–66.
44. Awawdeh, M.; Obeidat, M.; Al-Mohammad, M.; Al-Qudah, K.; Jaradat, R. Integrated GIS and remote sensing for mappinggroundwater potentiality in the Tulul al Ashaqif, Northeast Jordan. Arab. J. Geosci. 2013, 7, 2377–2392.
45. Saaty, T. Decision Making for Leaders: The Analytic Hierarchy Process for Decisions in a Complex World; RWS Publications: Pittsburgh,PA, USA, 2014.
46. Lentswe, G.; Molwalefhe, L. Delineation of potential groundwater recharge zones using analytic hierarchy process-guided GIS in the semi-arid Motloutse watershed, eastern Botswana. J. Hydrol. Reg. Stud. 2020, 28, 100674. [CrossRef]

47. Saaty TL. Basic theory of the analytic hierarchy process: how to make a decision. Revista de la Real Academia de Ciencias Exactas Fisicas y Naturales 1999; 93(4):395–423
48. Althuwaynee O.F, Pradhan B, Park HJ, Lee JH (2014) A novel ensemble decision tree-based Chi-squared Automatic Interaction Detection (CHAID) and multivariate logistic regression models in landslide susceptibility mapping. Landslides 2014; 11(6):1063–1078
49. Saaty TL (1992) The hierarchy: a dictionary of hierarchies. RWS Publications, Pittsburgh 496
50. Rahmati O, Nazari SA, Mahdavi M, Pourghasemi HR, Zeinivand H. Groundwater potential mapping at Kurdistan region of Iran using analytic hierarchy process and GIS. Arab J Geosci. 2014.
51. Mohammadi-Behzad HR, Charchi A, Kalantari N, Mehrabi NA, Karimi VH. Delineation of groundwater potential zones using remote sensing (RS), geographical information system (GIS) and analytic hierarchy process (AHP) techniques: a case study in the Leyla– Keynow watershed, southwest of Iran. Carbonates Evaporites 2019; 34(4):1307–1319
52. Rajasekhar M, Raju GS, Raju RS. Assessment of groundwater potential zones in parts of the semi-arid region of Anantapur District, Andhra Pradesh, India using GIS and AHP approach. Modeling Earth Sys Environ 2019; 5(4):1303–1317. [CrossRef]
53. Anbazhagan, S.; Ramasamy, S.; Das Gupta, S. Remote sensing and GIS for artificial recharge study, runoff estimation and planning in Ayyar basin, Tamil Nadu, India. Environ. Geol. 2005, 48, 158–170.
54. Opp, C. Bodenkörper. In Geographie—Physische Geographie und Humangeographie, 3rd ed.; Gebhardt, H., Glaser, R., Radtke, U.,Reuber, P., Vött, A., Eds.; Springer: Berlin, Germany, 2011; pp. 485–490.
55. Lakshmi, S.; Reddy, Y. Identification of groundwater potential zones using GIS and remote sensing. Int. J. Pure Appl. Math. 2018,119, 3195–3210.
56. Tolche, A. (2020). Groundwater potential mapping using geospatial techniques: A case study of Dhungeta-Ramis sub-basin, Ethiopia.Geol. Ecol. Landsc. 2020.
57. Muthumaniraja, C.K.; Anbazhagan, S.; Jothibasu, A.; Chinnamuthu, M. Remote Sensing and Fuzzy Logic Approach for Artificial Recharge Studies in Hard Rock Terrain of South India. In GIS and Geostatistical Techniques for Groundwater Science; Elsevier: Amsterdam, The Netherlands, 2019; pp. 91–112.
58. Wooding, R. A hydraulic model for the catchment stream problem. III Comparison with runoff observations. J. Hydrol. 1966, 4,21–37.
59. Kanagaraj, G.; Suganthi, S.; Elango, L.; Magesh, N. Assessment of groundwater potential zones in Vellore district, Tamil Nadu,India using geospatial techniques. Earth Sci. Inf. 2019, 12, 211–223.
60. Rajaveni, S.; Brindha, K.; Elango, L. Geological and geomorphological controls on groundwater occurrence in a hard rock region. Appl. Water Sci. 2015, 7, 1377–1389.
61. Gupta, M.; Srivastava, P. Integrating GIS and remote sensing for identification of groundwater potential zones in the hilly terrain of Pavagarh, Gujarat, India. Water Int. 2010, 35, 233–245.
62. Satapathy, I.; Syed, T. Characterisation of groundwater potential and artificial recharge sites in Bokaro District, Jharkhand (India), using remote sensing and GIS-based techniques. Environ. Earth Sci. 2015, 74, 4215–4232.

63. Magesh, N. S., Chandrasekar, N. & Soundranayagam, J. P. Delineation of groundwater potential zones in Teni district, Tamil Nadu, using remote sensing, GIS and MIFtechniques. Geosci. Front. 2012; 3, 189–196.
64. Hojati M, Mokarram M. Determination of a topographic wetness index using high-resolution digital elevation models. Eur J Geog 2016; 7(4):41–52
65. Pourali SH, Arrowsmith C, Chrisman N, Matkan AA, Mitchell D (2016) Topography wetness index application in flood-risk-based land use planning. Applied Spatial Anal Pol 2016; 9(1):39–54
66. Neilson BT, Cardenas MB, O'Connor MT, Rasmussen MT, King TV, Kling GW Groundwater flow and exchange across the land surface explain carbon export patterns in continuous permafrost watersheds. Geophys Res Lett 2018; 45(15):7596–7605
67. Saaty TL (1980) The analytic hierarchy process: planning, priority setting, resource allocation. McGraw-Hill, New York
68. Brunelli, M. Introduction to the Analytic Hierarchy Process; Springer: New York, NY, USA, 2015
69. Saaty, T. L. Decision making for leaders: the analytic hierarchy process for decisions in a complex world (RWS publications, 1990.
70. Brouwer, C.; Prins, K.; Kay, M.; Heibloem, M. Irrigation Water Management: Irrigation Methods; Training Manual No. 5. Food and Agriculture Organization of the United Nations, 1988.
71. Wang, J.; Huo, A.; Zhang, X. Prediction of the response of groundwater recharge to climate changes in Heihe river basin, China. Environ. Earth Sci. 2020; 79, 1–16.
72. Meixner J, Grimmer JC, Becker A, Schill E, Kohl T. Comparison of different digital elevation models and satellite imagery for lineament analysis: implications for identification and spatial arrangement of fault zones in crystalline basement rocks of the southern Black Forest (Germany). J Struct Geol 2018; 108:256–268
73. Raviraj, A.; Kuruppath, N.; Kannan, B. Identification of Potential Groundwater Recharge Zones Using Remote Sensing and Geographical Information System in Amaravathy Basin. J. Remote Sens. GIS 2017, 6, 213. [CrossRef
74. Kumar, V.; Mondal, N.; Ahmed, S. Identification of Groundwater Potential Zones Using RS, GIS and AHP Techniques: A CaseStudy in a Part of Deccan Volcanic Province (DVP), Maharashtra, India. J. Indian Soc. Remote Sens. 2020, 48, 497–511.
75. Rinderer M, Van Meerveld HJ, Seibert J. Topographic controls on shallow groundwater levels in a steep, pre-alpine catchment: when are the TWI assumptions valid? Water Res Res 2014; 50(7):6067–6080
76. Singh Sk Singh, C.K.; Mukherjee, S. Impact of land use and land cover change on groundwater quality in the lower Shiwalik hills: A remote sensing and GIS based approach. Cent. Eur. J. Geosci., 2010; 2, 124–131.
77. Fenta AA, Kifle A, Gebreyohannes T, Hailu G. Spatial analysis of groundwater potential using remote sensing and GIS-based multicriteria evaluation in Raya Valley, northern Ethiopia. Hydrogeol J 2015; 23(1):195–206
78. Li, P.; He, S.; Yang, N.; Xiang, G. Groundwater quality assessment for domestic and agricultural purposes in Yan'an City, Northwest China: Implications to sustainable groundwater quality management on the Loess Plateau. Environ. Earth Sci. 2018; 77, 775.

79. Orimoloye IR, Mazinyo SP, Nel W, Kalumba AM. Spatiotemporal monitoring of land surface temperature and estimated radiation using remote sensing: human health implications for East London, South Africa. Environ Earth Sci 2018; 77(3):77. [CrossRef].